nature cell biology

Developmental regulation of apical endocytosis controls epithelial patterning in vertebrate tubular organs

Alejo E. Rodríguez-Fraticelli[1], Jennifer Bagwell[2], Minerva Bosch-Fortea[1], Gaelle Boncompain[3], Natalia Reglero-Real[4], Maria J. García-León[4], Germán Andrés[5], Maria L. Toribio[4], Miguel A. Alonso[4], Jaime Millán[4], Franck Perez[3], Michel Bagnat[2,6] and Fernando Martín-Belmonte[1,6]

Epithelial organs develop through tightly coordinated events of cell proliferation and differentiation in which endocytosis plays a major role. Despite recent advances, how endocytosis regulates the development of vertebrate organs is still unknown. Here we describe a mechanism that facilitates the apical availability of endosomal SNARE receptors for epithelial morphogenesis through the developmental upregulation of *plasmolipin* (*pllp*) in a highly endocytic segment of the zebrafish posterior midgut. The protein PLLP (Pllp in fish) recruits the clathrin adaptor EpsinR to sort the SNARE machinery of the endolysosomal pathway into the subapical compartment, which is a switch for polarized endocytosis. Furthermore, PLLP expression induces apical Crumbs internalization and the activation of the Notch signalling pathway, both crucial steps in the acquisition of cell polarity and differentiation of epithelial cells. We thus postulate that differential apical endosomal SNARE sorting is a mechanism that regulates epithelial patterning.

To establish functional barriers, epithelial cells require the formation of polarized protein transport machineries[1]. Endocytosis is one of such processes that become highly polarized[2]. Interestingly, recent studies have described that immature epithelial sheets have a reduced rate of apical endocytosis that intensifies along development[3], which suggests that epithelial cells acquire the ability to internalize material specifically from the apical pole during differentiation. Indeed, apical protein endocytosis regulates polarity and proliferation in *Drosophila* epithelial cells[4,5]. These findings suggest that endocytosis could be regulated during development to coordinate epithelial morphogenesis[6]. However, the molecular mechanisms of this endocytic regulation in epithelial organ development have not been previously characterized. To unveil developmentally regulated proteins that may control the process of apical endocytosis we used the zebrafish gut morphogenesis model[7,8]. We describe the role of the protein Pllp, which is induced in the posterior segment of the zebrafish intestine during morphogenesis, and is required for the generation of a highly endocytic enterocyte population during gut differentiation. We also characterize the molecular mechanism controlling PLLP function during endocytosis using the three-dimensional (3D)-MDCK model. Using proteomics, we found that in 3D-MDCK cells PLLP interacts with EpsinR (EpsR), an AP1B-binding clathrin adaptor, which regulates the recycling of the endosomal SNAREs. Together, PLLP and EpsR are required for the sorting of endosomal SNAREs into the apical recycling compartment to properly feed the endocytic uptake of apical cargo. Finally, we demonstrate that the endocytic role of PLLP is essential for Crumbs (Crb) downmodulation and Notch activation to promote absorptive cell differentiation.

RESULTS

Pllp is induced during epithelial tube formation in zebrafish and localizes to a highly endocytic compartment of the midgut

Gut morphogenesis is a genetically regulated process. To unveil genes developmentally controlled during epithelial gut morphogenesis we used a screen strategy based on the isolation of epithelial cells from the zebrafish gut[8]. We identified *pllp* as one of the genes specifically induced during lumen formation and expansion (Fig. 1a). Pllp is a type III transmembrane protein of unknown function that belongs

[1]Department of Development and Differentiation, Centro de Biología Molecular 'Severo Ochoa', CSIC-UAM, Madrid 28049, Spain. [2]Department of Cell Biology, Duke University, Durham, North Carolina 27710, USA. [3]Department of Subcellular Structure and Cellular Dynamics, UMR144, Institut Curie, Paris 75005, France. [4]Department of Immunology and Cell Biology, Centro de Biología Molecular 'Severo Ochoa', CSIC-UAM, Madrid 28049, Spain. [5]Electron Microscopy Core, Centro de Biología Molecular 'Severo Ochoa', CSIC-UAM, Madrid 28049, Spain.
[6]Correspondence should be addressed to M.B. or F.M-B. (e-mail: m.bagnat@cellbio.duke.edu; fmartin@cbm.csic.es)

Received 24 July 2014; accepted 9 January 2015; published online 23 February 2015; DOI: 10.1038/ncb3106

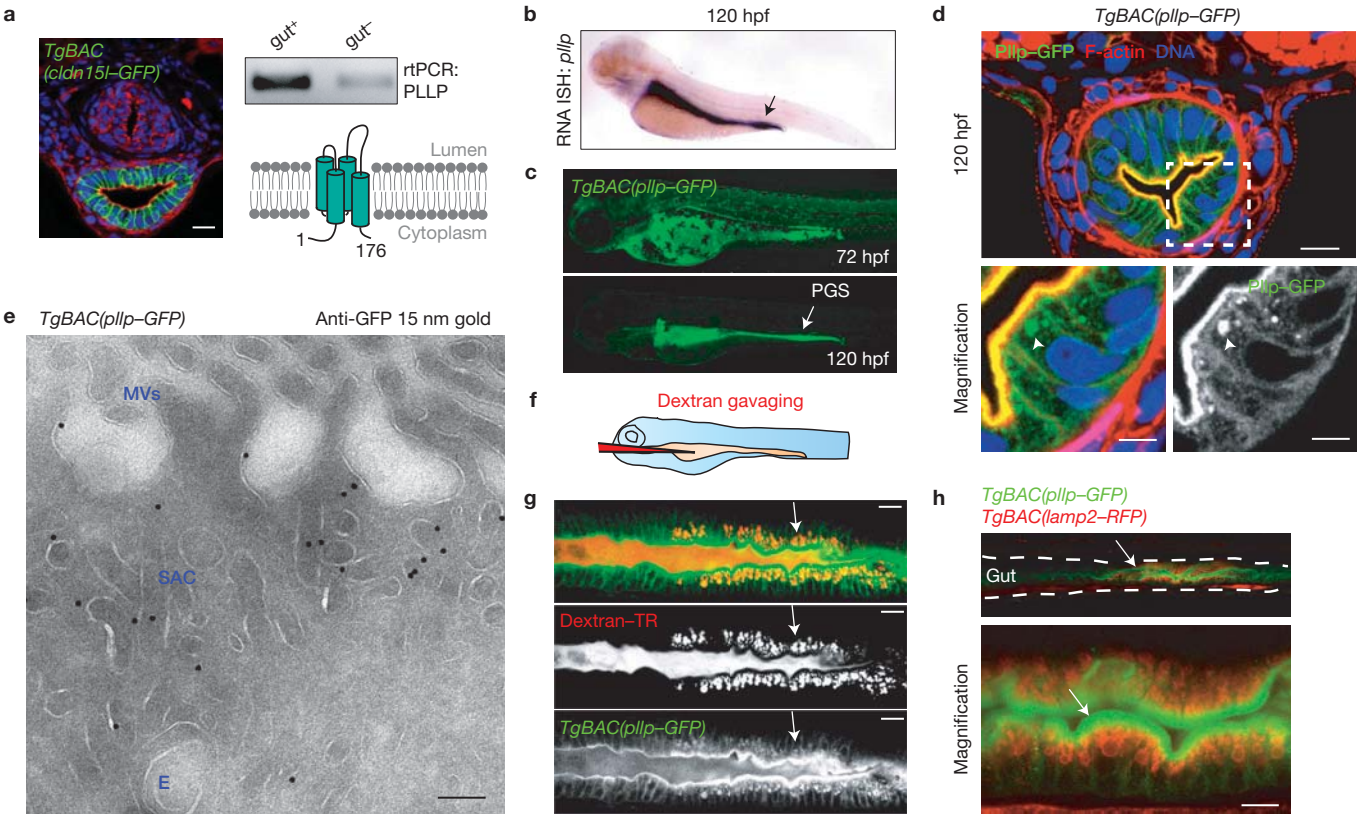

Figure 1 *pllp* expression is induced in endocytic enterocytes during development. (**a**) Identification of *pllp* as a gene induced during gut morphogenesis. Gut cells were FACS-sorted from *TgBAC(cldn15la–GFP)* zebrafish larvae and gut-specific cDNAs were cloned by real-time PCR (rtPCR). Bottom right, scheme of predicted PLLP structure showing N- and C-terminal cytoplasmic tails. Scale bar, 10 μm. (**b**) *In situ* hybridization (ISH) of *pllp* DIG-labelled RNA probe at 120 hpf. Arrow indicates the gut. (**c**) *TgBAC(pllp–GFP)* transgenic zebrafish larvae. A spacer–GFP sequence was recombined in place of the STOP codon using a zebrafish BAC clone carrying the full *pllp* gene. Note that the PGS contains a population of PLLP^{high} cells (arrow). (**d**) Transverse section of a *TgBAC*(*pllp–GFP*) larva posterior midgut, stained using phalloidin (which labels F-actin in apical microvilli, in red) and DAPI (for DNA, in blue). Arrowheads indicate apical endosomes. Scale bars, 10 μm (magnification, 5 μm). (**e**) Immunogold electron microscopy of *TgBAC*(*pllp–GFP*) using anti-GFP and protein-A gold particles. Most labelled protein (65%) resides in a subapical endosomal compartment (SAC), whereas 15% of the label localized to microvilli (MVs) and 13% was labelling more basal localized endosomes (E). Scale bar, 100 nm. (**f**) Gavaging of zebrafish larvae. Dextran–TR was force-fed by microinjection into anaesthetized 144 hpf larvae. (**g**) Dextran-gavaged *TgBAC*(*pllp–GFP*) larvae. *TgBAC*(*pllp–GFP*) larvae were gavaged with dextran–TR and analysed by live confocal microscopy 2 h post-gavaging. Note that the dextran is endocytosed only in the posterior midgut (arrow), where Pllp expression is higher. Scale bars, 20 μm. (**h**) *TgBAC(pllp–GFP)*; *TgBAC(lamp2–spRFP)* 144 hpf larvae analysed by live confocal microscopy. Lamp2 is localized specifically to the posterior midgut (arrows). Scale bar, 10 μm. Uncropped images of blots/gels are shown in Supplementary Fig. 5.

to the family of MARVEL-domain-containing proteins associated with vesicle trafficking and membrane fusion[9]. We corroborated the expression of *pllp* in the gut using RNA *in situ* hybridization (Fig. 1b and Supplementary Fig. 1A). *pllp* is expressed in the hatching gland and the pronephric duct as early as 48 hours post-fertilization (hpf), and is highly enriched in the gut at 72 hpf and 120 hpf (Fig. 1b, arrows, and Supplementary Fig. 1A). To analyse the subcellular localization of the Pllp protein, we used bacterial artificial chromosome (BAC) recombineering[10] to generate a BAC expressing Pllp–GFP and obtained stable transgenic animals *TgBAC(pllp–spGFP)*. We found that Pllp expression is highly induced in a specific segment of the posterior midgut (PGS) at 120 hpf (Fig. 1c and Supplementary Fig. 1B). Pllp–GFP localizes to the apical region of intestinal epithelial cells (IECs), with a small population associated with internal membranes (Fig. 1d, arrowheads, and Supplementary Fig. 1C). To further evaluate the subcellular localization of the protein, we performed anti-GFP immunogold electron microscopy in gut sections (Fig. 1e). Most Pllp–GFP (65%) localized to small tubules and vesicles (about 70–100 nm wide) present in the first 300 nm below the apical membrane, with a small fraction of PLLP also distributed both to the apical microvilli and to more basal endosomes. This polarized localization of Pllp suggests a function associated with the apical endocytic pathway.

Therefore, we next analysed whether Pllp is involved in apical endocytosis in the zebrafish gut by using microgavaging to deliver endocytic tracers directly into the intestinal lumen[11] (Fig. 1f). Interestingly, gavaged dextran–Texas red (TR) was specifically internalized in the posterior midgut in 144 hpf *TgBAC(pllp–spGFP)* larvae where Pllp is enriched (Fig. 1g, arrows). Furthermore, we observed that Lamp2, a late endosomal marker, is specifically enriched in Pllp-positive cells (Fig. 1h, arrows). Thus, Pllp is a marker of highly endocytic enterocytes of the posterior midgut at the onset of intestinal differentiation.

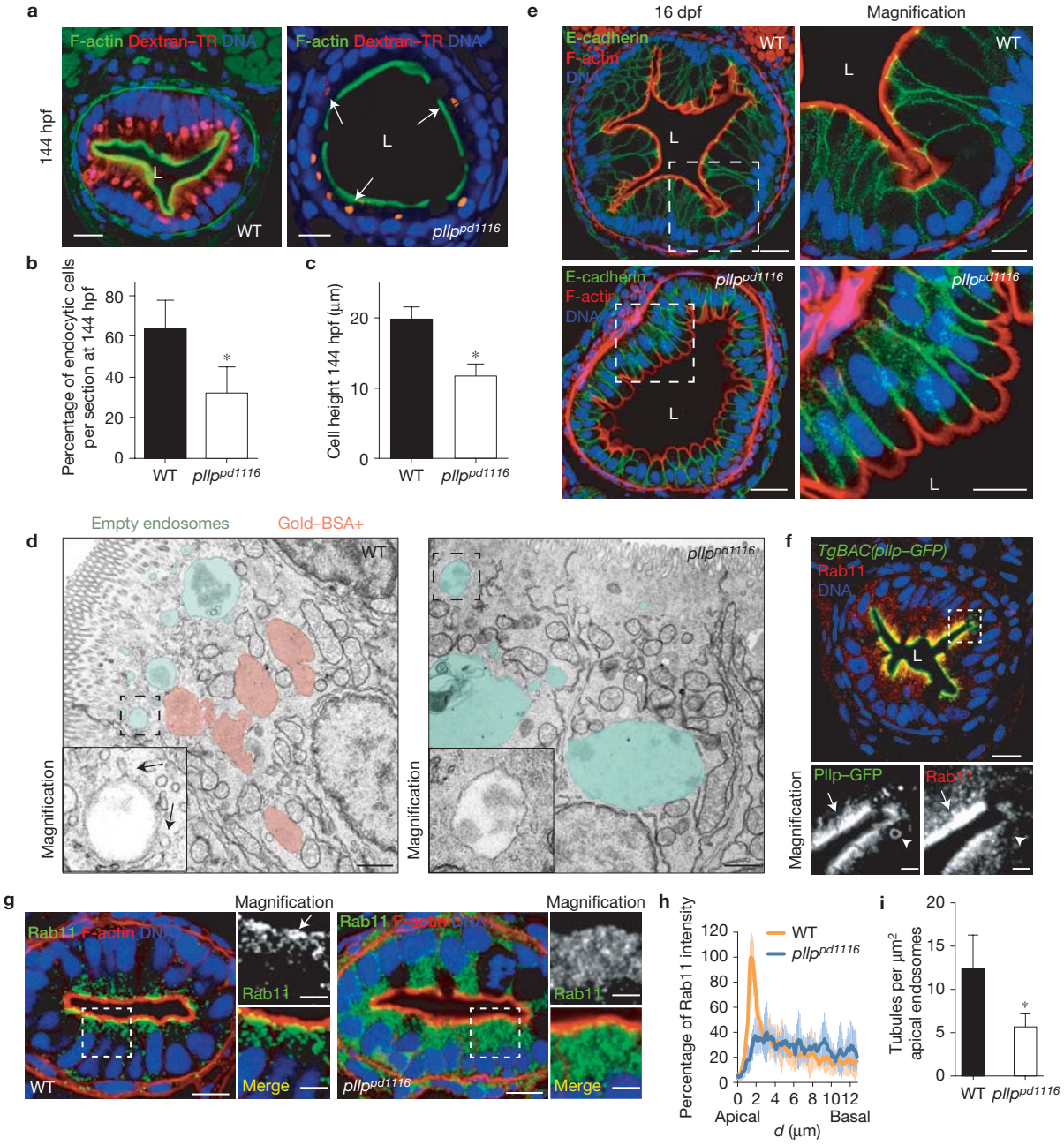

Figure 2 Pllp is required for apical endocytosis and epithelial morphogenesis in the zebrafish gut. (**a**) Endocytosis of dextran in *pllp*^{pd1116} mutants. Posterior midgut sections of dextran-gavaged (red) 144 hpf larvae were labelled with phalloidin (green) and DAPI (blue). Arrows indicate remaining cells that are able to endocytose dextran in the mutant. L, lumen. Scale bar, 10 μm. (**b**) Quantification of endocytic cells in *pllp*^{pd1116} mutants. Data are mean ± s.d. percentage of endocytic cells (WT, 63.9 ± 8.2%; *pllp*^{pd1116} 32 ± 9,3%; $n = 10$ sections from 5 WT and 6 mutant fish, randomly selected from 3 independent gavaging experiments; $^{*}P < 0.005$ (Student's *t*-test)). (**c**) Quantification of cell height in *pllp*^{pd1116} mutants. Data are mean ± s.d. cell height in μm (WT, 19.7 ± 1.8 μm; *pllp*^{pd1116}, 11.7 ± 1.7 μm; $n = 10$ sections from 7 WT and 6 mutant fish, randomly selected from 3 independent experiments; $^{*}P < 0.005$ (Student's *t*-test)). (**d**) Electron microscopy sections of *pllp*^{pd1116} mutant fish gavaged with dextran and BSA-gold (15 nm). BSA-positive compartments (red) and BSA-empty endosomes (green) are coloured. Scale bars, 1 μm. (**e**) Epithelial morphology is disrupted in *pllp*^{pd1116} juveniles. Larvae were raised in 1 l tanks, fixed at 16 dpf, sectioned and stained with the anti-E-cadherin antibody (green), phalloidin (red) and DAPI (blue). L, lumen. Scale bars, 20 μm (magnification, 10 μm). (**f**) PLLP and Rab11a co-localization in zebrafish enterocytes. *TgBAC(pllp–GFP)* 144 hpf guts are labelled with anti-Rab11 (red) and DAPI (blue). Arrows indicate co-localization. Arrowheads indicate Rab11-negative PLLP endosomes. L, lumen. Scale bars, 10 μm (magnification, 5 μm). (**g**) Rab11 localization in WT and *pllp*^{pd1116} 96 hpf larval guts. Larvae were fixed, sectioned and stained with anti-Rab11 (green), phalloidin (red) and DAPI (blue). Arrow indicates the subapical compartment. Scale bars, 10 μm (magnification, 5 μm). (**h**) Quantification of Rab11 localization in **g**. Fluorescent intensity linear profiles were drawn perpendicular to the centre of the apical plasma membrane (0 is the peak of apical F-actin staining). Data are averaged linear profiles ± s.d. ($n = 16$ WT and 12 mutant cells from 3 independent experiments). (**i**) Quantification of tubulating membranes in WT and *pllp*^{pd1116} larvae. The number of connected tubular structures was counted in every apical endosome (>300 nm diameter). For every endosome, the endosomal surface was determined as a function of perimeter × slice depth. Results are represented as number of tubules counted per endosomal surface unit (in μm^2) ± s.d. ($n = 5$ WT and 5 mutant fish pooled from 2 independent experiments; $^{*}P < 0.05$ (Student's *t*-test)).

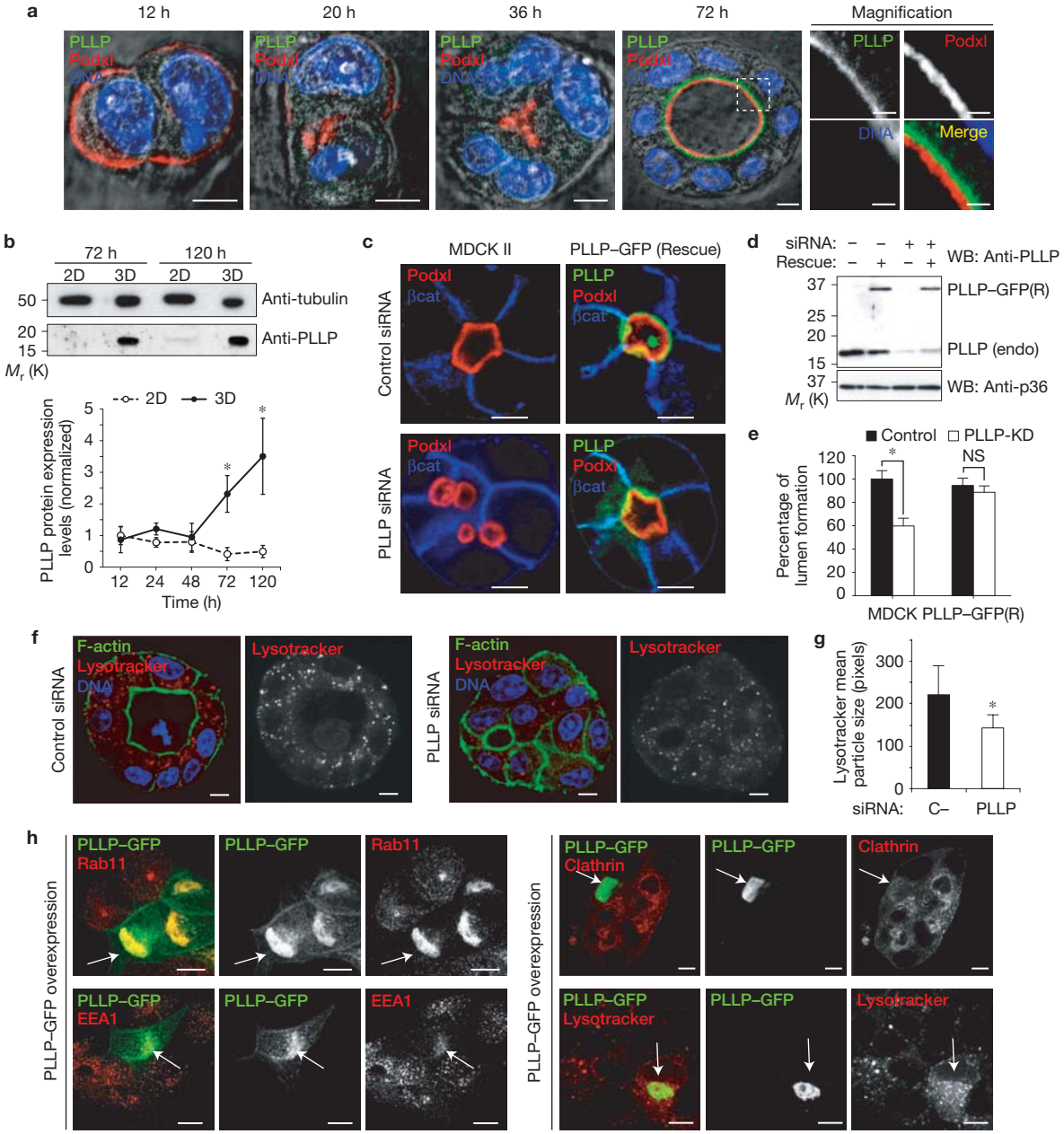

Figure 3 PLLP is required for epithelial morphogenesis and endosomal maturation in MDCK cysts. (**a**) Expression of PLLP in MDCK cysts at different time points. MDCK cells were grown to form cysts and fixed after 12, 20, 36 and 72 h. MDCK cysts were labelled with anti-PLLP antibody (green), anti-Podxl (red) and DNA (blue) and analysed by confocal microscopy using differential interference contrast. Scale bars, 5 μm (magnification, 2 μm). (**b**) Expression of PLLP in MDCK cysts and monolayers at different time points. MDCK cells were grown to form cysts and lysed after 12, 24, 48, 72 and 120 h. Western blot analysis was performed to quantify PLLP protein levels at different time points (bottom graph). Data represent mean ± s.d. ($n = 4$ independent western blots; $^*P < 0.005$ (Student's *t*-test); statistics source data can be found in Supplementary Table 3). (**c**) PLLP-KD phenotype in MDCK cysts, and phenotype rescue. WT MDCK cells or MDCK cells stably expressing siRNA-resistant PLLP–GFP(R) protein were transfected with control or PLLP-specific siRNAs and grown to form cysts. MDCK cysts were fixed and labelled with anti-Podxl (red), anti-β- catenin (blue) and analysed by confocal microscopy. Scale bars, 5 μm. (**d**) Western blot of PLLP KD and rescue experiments. Whole-cell lysates were prepared and analysed by western blotting using anti-PLLP antibody and anti-p36 as a loading control. (**e**) Quantification of PLLP-KD phenotype and rescue. Measurements are normalized to WT MDCK cells (control) and expressed as mean ± s.d. percentage relative to control single-lumen-forming cysts (control, 100 ± 7.2%, siRNA PLLP, 59.8 ± 6.6%, PLLP(R)-control, 94.5 ± 6.3%, PLLP(R)-siRNA PLLP, 88.7 ± 5.4%; $n = 3$ independent transfection experiments; $^*P < 0.005$, NS, not significant (Student's *t*-test); statistics source data can be found in Supplementary Table 3). (**f**) Endosomal acidification defect in PLLP-KD cysts. MDCK cells transfected with control or PLLP-specific siRNAs were grown to form cysts for 72 h, labelled with Lysotracker-red for 2 h, and then fixed. MDCK cysts were also labelled with phalloidin (green) and ToPRO3 (DNA, blue) and analysed by confocal microscopy. Scale bars, 5 μm. (**g**) Quantification of endosomal acidification defect in **f**. Data are represented as mean ± s.d. particle size in square pixels ($n = 17$ control and 18 PLLP-KD cysts selected randomly from 4 independent siRNA experiments; $^*P < 0.01$ (Student's *t*-test)). (**h**) Overexpression of PLLP–GFP in MDCK monolayers. MDCK cells transiently transfected with PLLP–GFP (green) were analysed at 48 h and labelled with anti-Rab11, anti-EEA1, anti-Clathrin and Lysotracker (red). Arrows indicate endosomal aggregates in PLLP-overexpressing cells. Scale bars, 5 μm. Uncropped images of blots/gels are shown in Supplementary Fig. 5.

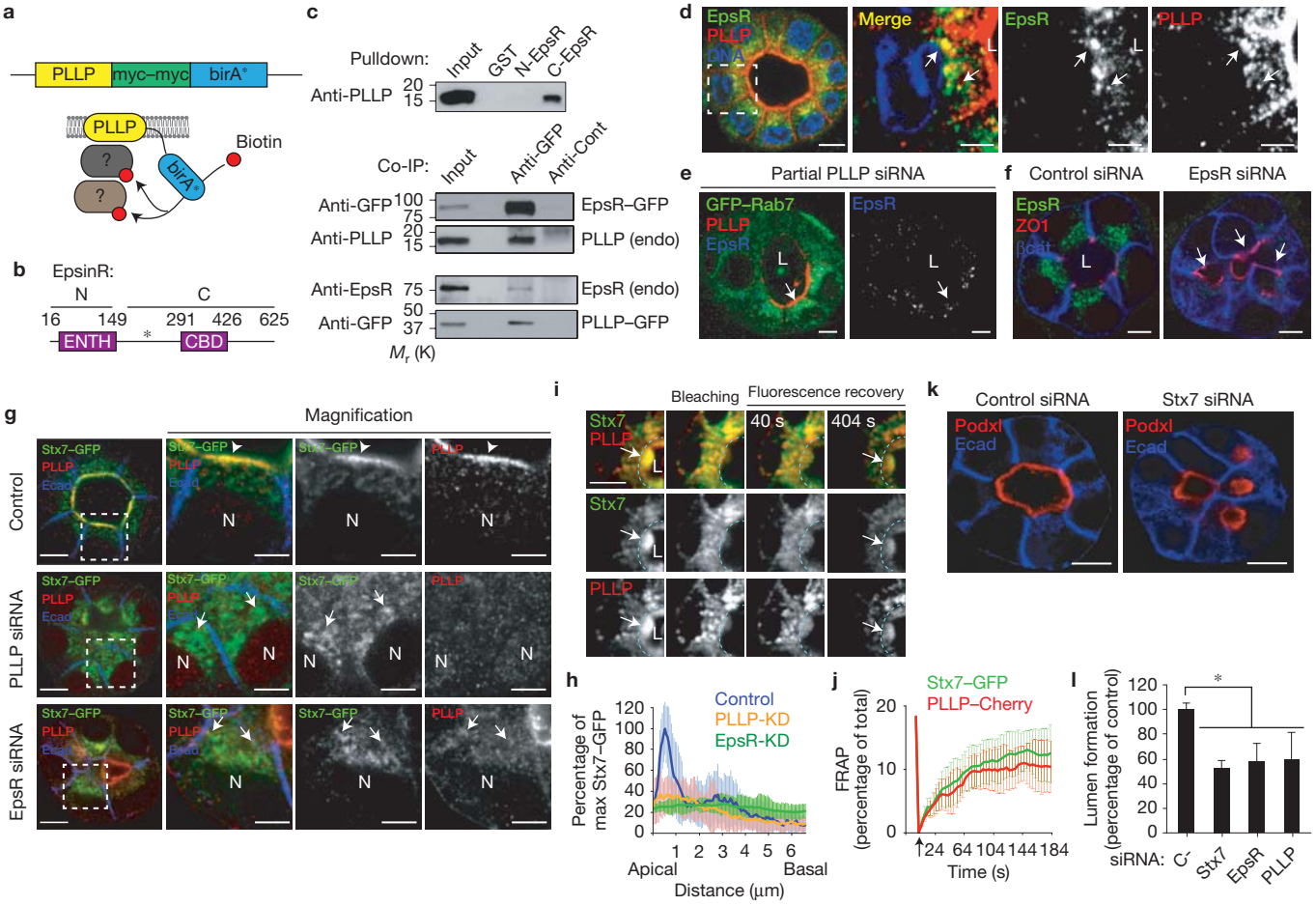

Figure 4 EpsR/PLLP mediate polarized apical sorting of endosomal SNARE Stx7. (**a**) *In vivo* bioID assay to identify PLLP-interacting proteins. (**b**) Protein structure of EpsR. EpsR was biotinylated in a specific segment of the C-terminal region (asterisk). (**c**) Pulldown and co-immunoprecipitation of endogenous PLLP and EpsR using GST-tagged EpsR fragments, EpsR–GFP or PLLP–GFP. (**d**) Endogenous EpsR and PLLP localization. MDCK cysts were labelled with anti-PLLP antibody (red), anti-EpsR (green) and DNA (blue). Arrows indicate PLLP and EpsR co-localizing in perinuclear endosomes. Scale bars, 5 μm (magnification, 2 μm). (**e**) Disrupted Rab7 and EpsR localization in PLLP-KD. MDCK cells stably expressing Rab7–GFP were transfected with PLLP siRNAs, grown in cysts and labelled with anti-PLLP (red) and anti-Epsin-R (blue). Arrow indicates non-depleted cells. Scale bars, 5 μm. (**f**) Phenotype of EpsR-KD. MDCK cells were transfected with control or EpsR-specific siRNAs, grown in cysts and labelled with anti-EpsR (green), anti-ZO1 (red) and anti-β catenin (blue). L, lumen. Arrows indicate multiple lumina. Scale bars, 5 μm. (**g**) Stx7 localization in PLLP-KD and EpsR-KD MDCK cysts. MDCK cells stably expressing Stx7–GFP were transfected with control, PLLP or EpsR-specific siRNAs, grown in cysts and labelled with anti-PLLP (red) and anti-E-cadherin (blue). Arrowheads indicate PLLP/Stx7 co-localization. Arrows indicate PLLP/Stx7 in perinuclear endosomes. Scale bars, 5 μm. (**h**) Quantification of Stx7 localization in **g**. GFP–Stx7 linear profiles were drawn perpendicular to the centre of the apical plasma membrane. Data represented are averaged linear profiles ± s.d. ($n = 19$ control and 27 PLLP-KD cells randomly selected from 4 independent experiments). (**i**) Stx7 and PLLP FRAP assay. MDCK cells expressing PLLP–Cherry were transfected with Stx7–GFP and grown in cysts for 72 h. Photobleaching was performed inside the region outlined by the dashed line, and cysts were imaged every 4 s. Scale bars, 5 μm. (**j**) Quantification of FRAP assay. Data are mean ± s.d. percentage of total fluorescence intensity inside the photobleached region ($n = 6$ cysts from 3 independent FRAP experiments). (**k**) Phenotype of Stx7-KD. MDCK cells transfected with control or Stx7-specific siRNAs were grown in cysts and labelled with anti-Podxl (red) and anti-E-cadherin (blue). Scale bars, 5 μm. (**l**) Quantification of phenotypes in PLLP-KD, EpsR-KD and Stx7-KD MDCK cysts. Measurements are expressed as mean ± s.d. percentage (relative to control) of single-lumen-forming cysts in 3 different independent experiments (control, 100 ± 5.3%; Stx7-KD, 52.3 ± 6.4%; EpsR-KD, 58.06 ± 14.5%; PLLP-KD, 59.7 ± 22.1%; $n = 3$ independent transfection experiments; $^*P < 0.005$ (Student's *t*-test), statistics source data can be found in Supplementary Table 3). Uncropped images of blots/gels are shown in Supplementary Fig. 5.

Pllp is required for apical endocytosis and endosomal maturation in the zebrafish posterior midgut

To analyse whether Pllp is required for apical endocytosis in the gut, we generated a mutant allele using TAL-effector nucleases[12] (TALENs). We identified one allele that contained an insertion/deletion (*pd1116*), giving rise to a frame-shift mutation and an early STOP codon, which truncates 85% of the protein structure (Supplementary Fig. 1D). Homozygous *pllp*^{pd1116} larvae develop normal early gut morphology and intestinal cell numbers (Supplementary Fig. 1E,F), but present marked defects in the number of endocytic cells and the amount of dextran that was internalized in the PGS (Fig. 2a,b). In addition, at 144 hpf, *pllp*^{pd1116} IECs are significantly shorter than the wild type (WT; Fig. 2c and Supplementary Fig. 1G), a phenotype also observed in *pllp* morphants (Supplementary Fig. 1H–J), and present stubbier microvilli (Supplementary Fig. 1K). To more precisely evaluate the internalization defects, we gavaged *pllp*^{pd1116} larvae with dextran–TR

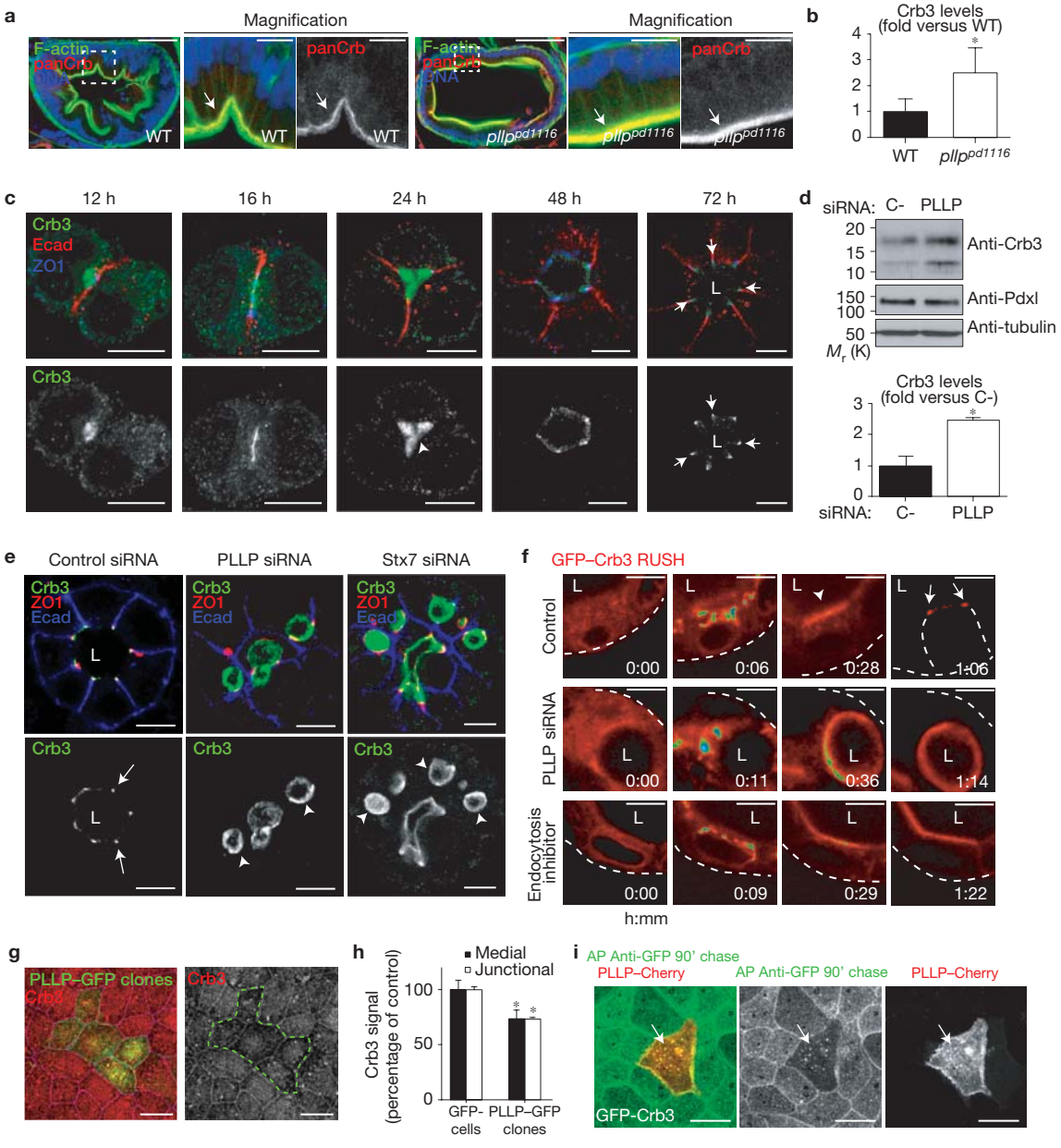

Figure 5 PLLP regulates Crb endocytosis. (**a**) Crb localization in WT and *pllp*^{pd1116} mutant 144 hpf larvae. Sections were stained with anti-panCrb (red), phalloidin (green) and DAPI (blue). Arrows indicate Crb localization at apical membrane. Scale bars, 20 μm (magnification, 10 μm). (**b**) Quantification of Crb levels in **a**. Data are represented as average fold-increase ± s.d. (WT, 1.00 ± 0.50 fold; *pllp*^{pd1116}, 2.50 ± 0.96 fold; $n = 6$ WT and 6 mutant fish from 3 independent experiments; $^{*}P < 0.005$ (Student's *t*-test)). (**c**) Localization of endogenous Crb3. MDCK cysts were fixed and labelled with anti-Crb3 (green), anti-ZO-1 (blue) and anti-E-cadherin (red). Arrowhead indicates apical Crb3. Arrows indicate suprajunctional Crb3. Scale bars, 5 μm. (**d**) Crb3 protein levels in PLLP-KD cysts. Data are expressed as mean ± s.d. fold-increase versus control (control, 1 ± 0.35 fold; PLLP-KD, 2.31 ± 0.13 fold; $n = 3$ extracts from 3 independent experiments, $^{*}P < 0.005$ (Student's *t*-test), statistics source data can be found in Supplementary Table 3). (**e**) Localization of endogenous Crb3 in PLLP-KD and Stx7-KD cysts. MDCK cells transfected with control, PLLP or Stx7-specific siRNAs were grown in cysts and labelled with anti-Crb3 (green), anti-ZO-1 (red) and anti-E-cadherin (blue). L, lumen. Arrowheads indicate apical Crb3. Arrows indicate suprajunctional Crb3. Scale bars, 5 μm. (**f**) Videomicroscopy of RUSH-Crb3a. RUSH-Crb3a MDCK cells were transfected with control or PLLP siRNA and grown to form cysts. At 72 h, biotin was added and cysts were recorded every minute until steady state. For endocytosis inhibition, cysts were treated with dynasore after biotin addition. Arrowheads indicate apical membrane. Arrows indicate tight junctions. Dashed lines mark the basal contour of the cysts. L, lumen. Scale bars, 5 μm. (**g**) Downmodulation of Crb3 in PLLP–GFP clones. PLLP–GFP-transfected cells were grown as monolayers for 4 days mixed with control MDCK cells, fixed and labelled with anti-Crb3 (red). The dashed line indicates the PLLP–GFP-expressing clone. Scale bars, 10 μm. (**h**) Quantification of **g**. Medial and junctional Crb3 staining was measured as mean percentage of control fluorescence intensity ± s.d. (GFP-neg, 100 ± 8.3%; PLLP–GFP, 73.6 ± 7.7%; $n = 20$ PLLP–GFP cells and 61 GFP-neg cells from 3 independent transfection experiments, $^{*}P < 0.01$ (Student's *t*-test)). (**i**) Pulse-chase endocytosis of GFP–Crb3a. MDCK cells stably expressing GFP–Crb3a were transfected with PLLP–Cherry. After 24 h, the apical surface of the cells was incubated with anti-GFP to label Crb3 at 4 °C, washed, and cells were returned to 37 °C for 90 min. Then, cells were fixed and stained with anti-rabbit-Alexa647 (green). Images are maximum *z*-stack projections. Arrows indicate endocytosed apical GFP–Crb3a. Scale bars, 10 μm. Uncropped images of blots/gels are shown in Supplementary Fig. 5.

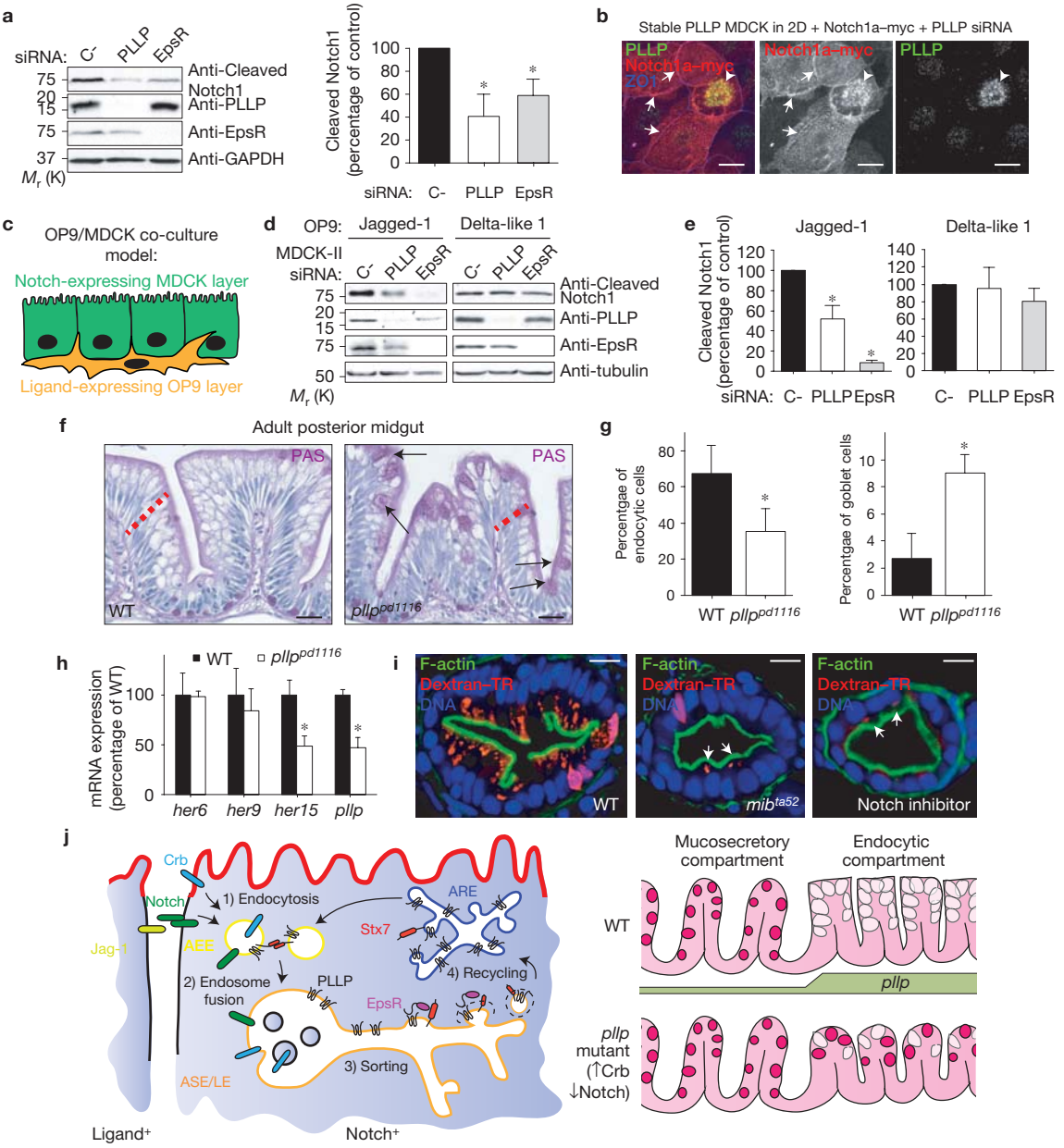

Figure 6 PLLP is required for Notch signalling. (**a**) Notch activation in PLLP-KD and EpsR-KD cysts. Cleaved Notch1 (NICD) protein levels were analysed by western blotting. Data are mean ± s.d. as percentage of control (PLLP, 41 ± 19%, EpsR; 59 ± 14%, $n = 3$ extracts from 3 independent experiments, $^*P < 0.05$ (Student's t-test), statistics source data can be found in Supplementary Table 3). (**b**) Notch localization in PLLP-KD cells. Cells were transfected with Notch1a–myc and PLLP siRNA and labelled with anti-myc (red), anti-PLLP (green) and anti-ZO1 (blue). Arrows indicate junctional Notch1a–myc in PLLP-depleted cells. Arrowheads indicate internal PLLP and Notch1a–myc co-localization in non-depleted cells. Scale bars, 10 μm. (**c**) MDCK-II/OP9 co-culture system for ligand-induced Notch1 transactivation assays. (**d**) Effect of PLLP-KD or EpsR-KD on ligand-specific Notch1 transactivation. MDCK cells stably expressing Notch1a–myc were transfected with control, PLLP or EpsR-specific siRNAs and cultured with OP9 cells expressing Jagged-1 or Delta-like-1 and analysed by western blotting. (**e**) Quantification of Notch1 activity in **d**. Data are mean ± s.d.% of control cleaved Notch1 (PLLP-KD, 57.5 ± 17.5%; EpsR-KD, 8.2 ± 5.6%; $n = 3$ extracts from 3 independent experiments, $^*P < 0.05$ (Student's t-test), statistics source data can be found in Supplementary Table 3). (**f**) Intestinal morphology in adult $pllp^{pd1116}$ posterior guts. Sections were stained with PAS (purple). Arrows indicate goblet cells. Red bars are placed to compare cell height. Scale bars, 20 μm. (**g**) Quantification of endocytic cells and goblet cells. Data are expressed as mean ± s.d. percentage of total cells from 9 crypts per animal (endocytic cells: WT, 67.3 ± 15.5%; $pllp^{pd1116}$, 35.3 ± 12.4%; goblet cells: WT, 2.7 ± 1.8%; $pllp^{pd1116}$ 9.0 ± 1.3%; $n = 6$ WT, 6 mutant fish from 2 independent experiments; $^*P < 0.005$ (Student's t-test)). (**h**) Expression of Notch-target *hes-related* genes in WT and $pllp^{pd1116}$ adult guts. Data are mean ± s.d. percentage of control expression ($n = 3$ extracts from 3 independent experiments; $^*P < 0.01$ (Student's t-test), statistics source data can be found in Supplementary Table 3). (**i**) Dextran endocytosis in Notch-inhibited larvae. DMSO (control) or 100 μM DAPT (Notch inhibitor)-treated larvae and $mib1^{ta52b}$ mutants were dextran-gavaged (red) and stained with phalloidin (green) and DNA (blue). Arrows indicate the few remaining cells that are able to endocytose dextran. Scale bars, 10 μm. (**j**) Model. Apical endosomal SNAREs, that is, Stx7, are polarized. In mature sorting endosomes Pllp recruits EpsR, which binds Stx7 to recycle it specifically to the apical pole through the ARE. The patterned expression of Pllp in the zebrafish intestine regulates Crb and Notch receptor endocytosis and results in functional patterning of the midgut by promoting terminal differentiation of absorptive endocytic cells. Uncropped images of blots/gels are shown in Supplementary Fig. 5.

and BSA-conjugated 15 nm gold for ultrastructural analysis. IECs of *pllp*^{pd1116} larvae present alterations in apical endosome numbers and size distribution, and negligible levels of apical BSA–gold endocytosis compared with WT (Fig. 2d and Supplementary Fig. 1G, arrows, and Supplementary Fig. 1L). At later time points, juvenile *pllp*^{pd1116} mutants (75%) present disrupted intestinal folds and a 1.4-fold expansion in apical membrane size (Fig. 2e and Supplementary Fig. 1M), a phenotype resembling previous observations in *Drosophila* mutants with disrupted apical endocytosis[5]. The survival of *pllp*^{pd1116} mutants raised with a limited food supply was highly compromised compared with WT juveniles, suggesting that Pllp is necessary for efficient nutrient absorption (Supplementary Fig. 1N). We validated the specificity of phenotypes by crossing *pllp*^{pd1116} mutants to *TgBAC(pllp–GFP)* heterozygous animals. Pllp–GFP expression almost completely rescued both the endocytic and the cell-height phenotypes of the *pllp*^{pd1116} mutation, indicating that the lack of *pllp* expression in the mutants is the specific cause of the observed defects in IECs and that the fusion protein is functional (Supplementary Fig. 1O,P). To summarize, these results indicate that Pllp is required for apical endocytosis and epithelial morphogenesis in the gut and suggest a function in regulating terminal epithelial differentiation of posterior gut enterocytes.

PLLP regulates formation of apical recycling endosomes

The subapical localization of PLLP suggests its association with apical recycling endosomes (AREs), which are required for the recycling of endocytosed receptors back to the plasma membrane[13]. Endogenous Rab11, an ARE marker, partially co-localized with subapical Pllp (Fig. 2f, arrows, $r = 0.64 \pm 0.09$). We observed that in *pllp*^{pd1116} mutants Rab11 is mislocalized throughout the cytoplasm in posterior gut IECs, before any morphogenetic defects arise (Fig. 2g,h and Supplementary Fig. 1Q), suggesting that Pllp is required for the formation or maintenance of a polarized ARE compartment, and possibly for protein recycling at the onset of epithelial morphogenesis. In addition, electron micrographs of IECs revealed that *pllp*^{pd1116} mutants presented a 2.6-fold decrease in the number of recycling/sorting tubules in apical endosomes compared with WT (Fig. 2d, insets, 2i and Supplementary Fig. 2A). In conclusion, Pllp is required for polarized Rab11 distribution in epithelial cells, suggesting that Pllp is required for the formation or maintenance of the ARE compartment, and possibly for protein recycling from apical sorting endosomes during epithelial morphogenesis.

PLLP is required for epithelial morphogenesis and endosomal maturation in MDCK cysts

To dissect more precisely the molecular function of PLLP we used the 3D-MDCK model system, which aptly recapitulates epithelial morphogenesis *in vitro*[14]. PLLP expression increases during lumen formation and localizes to the subapical compartment in 3D-MDCK cells (Fig. 3a,b). We also observed a similar pattern of expression in sections of mouse small intestine and kidney (Supplementary Fig. 2B,C), mimicking the subcellular localization and expression patterns observed in zebrafish. This common pattern of subcellular localization in epithelial tubes suggests a potential similar role in all of these tissues. Consistently, silencing of PLLP (PLLP-KD) results in morphogenetic defects (Fig. 3c–e and Supplementary Fig. 2D,E) and endolysosomal function defects (Fig. 2f,g). Furthermore, PLLP also partially co-localizes with Rab11 ($r = 0.73 \pm 0.12$) and PLLP-KD disrupts ARE polarization (Supplementary Fig. 2F,G). These results suggest a conserved role for PLLP in ARE polarization and endosomal maturation. Next, we tested whether PLLP overexpression is sufficient to enhance formation of Rab11 endosomes. Overexpression of PLLP–GFP in monolayers of MDCK cells (2D) induces the formation of an enlarged Rab11-positive compartment, which co-localizes with early endosomal markers and induces the formation of acidic endosomes (Fig. 3h). This PLLP–GFP compartment consisted of clusters of vesicles that resembled ARE tubule vesicles (Supplementary Fig. 2H). The *TgBAC(pllp–GFP)pd1114* line, which overexpresses Pllp–GFP, presents a similar phenotype (Supplementary Fig. 2I). In summary, these experiments indicate that PLLP is required for endosomal maturation and ARE polarization, and furthermore that PLLP expression is sufficient to expand the ARE, and enhance formation of lytic acidic endosomes.

PLLP interacts with EpsR to sort endosomal SNAREs to the recycling compartment

To characterize the molecular mechanism associated with PLLP function, we devised an *in vivo* biotinylation assay (bioID) of PLLP-proximal proteins (Fig. 4a). We uncovered 42 proteins likely to interact with PLLP in 3D-MDCK cells, including 20 proteins with trafficking functions and 9 SNARE proteins or SNARE regulators (Supplementary Tables 1 and 2). We identified Clint-1 (also known as Epsin-4 or EpsR, and hereafter termed EpsR) as the principal interacting partner of PLLP (Fig. 4b). EpsR belongs to the Epsin family of membrane-tubulating proteins and it is required for retrograde transport from late endosomes[15–17]. The amino-terminal ENTH domain of EpsR has been described to interact with several cargoes, including endosomal SNAREs, and is required for SNARE recycling[18–20]. We confirmed the interaction between endogenous PLLP and the carboxy-terminal domain of EpsR (Fig. 4c) and found that EpsR and PLLP partially co-localize in internal endosomes (Fig. 4d, arrows, and Supplementary Fig. 3A, arrows, $r = 0.61 \pm 0.08$). PLLP-KD cells present a dispersed and decreased staining of both EpsR and Rab7 (Fig. 4e and Supplementary Fig. 3B) suggesting that PLLP is required for EpsR endosomal localization and maturation of degradative endosomes. EpsR silencing phenocopies PLLP-KD (Fig. 4f,l, and Supplementary Fig. 3C,D) and inhibits PLLP gain-of-function phenotypes (Supplementary Fig. 3E), indicating that EpsR binding to PLLP is required for the formation of apical Rab11-positive endosomes. Interestingly, the *Drosophila* EpsR homologue, *Liquid-facets related* (*lqfR*) is a regulator of epithelial cell morphology and regulates cell height in the follicle cells of the egg chamber[21,22], which, together with our results, suggests that EpsR function in epithelial morphogenesis is conserved across bilateria.

Next, we investigated one of the canonical cargoes of EpsR, Syntaxin-7 (Stx7; ref. 18), which was also identified in our bioID assay (Supplementary Table 2). Stx7 is highly polarized to the subapical endosomal compartment in 3D-MDCK (Fig. 4g) and mouse intestine (Supplementary Fig. 3F). Furthermore, Stx7 and PLLP co-localize in the subapical compartment (Fig. 4g, arrowheads, $r = 0.83 \pm 0.05$), and interact in these membrane domains as we observed using a probe-ligation assay[23] (Supplementary Fig. 3G,H). Next, we addressed

whether Stx7 subapical localization requires PLLP and EpsR. We found that silencing either PLLP or EpsR mislocalized Stx7 from the subapical compartment (Fig. 4g,h). FRAP (fluorescence recovery after photobleaching) analysis of subapical endosomes revealed similar recovery kinetics for both proteins (k_{off} Stx7, 0.022 s^{-1}; k_{off} PLLP, 0.026 s^{-1}), suggesting that they traffic in the same carriers to the subapical compartment (Fig. 4i,j, Supplementary Video 1). Moreover, we found that Stx7 silencing phenocopies PLLP and EpsR-KD (Fig. 4k,l and Supplementary Fig. 3I–L). Consistently, *pllp*^{pd1116} larvae showed a scattered distribution of Stx7, recapitulating PLLP-KD in MDCK cysts (Supplementary Fig. 3M).

Together these results indicate that endosomal SNAREs are polarized in the subapical compartment in epithelial cells and recycled back to the apical pole from sorting/late endosomes by interacting with PLLP and EpsR. These data also imply that formation of Rab11 endosomes depends on the maintenance of apical endosomal fusion and a cyclic dependence of both apical endocytosis and the recycling of the SNARE fusion machinery.

PLLP regulates Crb endocytosis and Notch signalling during epithelial morphogenesis

Our data suggest the possibility that PLLP levels could modulate endocytosis and degradation of apical protein receptors. Crb is a master regulator of epithelial morphogenesis and is regulated by endocytosis[24–26]. *In vivo*, *pllp*^{pd1116} mutants exhibited higher levels of Crumbs (Fig. 5a,b). In 3D-MDCK cells, Crumbs3 (Crb3) becomes progressively restricted to tight junctions (Fig. 5c and Supplementary Fig. 4A), correlating with the timing of PLLP induction, whereas PLLP-KD cells present Crb3 mislocalized to the apical plasma membrane and higher total levels of Crb3 (Fig. 5d,e, arrowheads, and Supplementary Fig. 4A–C). Crb3 mis-sorting could be explained by a defect in protein sorting to the tight junctions or by a defect in endocytosis at the apical plasma membrane. To dynamically address GFP–Crb3(a) localization we used the RUSH system[27] (Supplementary Video 2). GFP–Crb3 is secreted first at the apical plasma membrane from where it then relocalizes to the tight junctions (Fig. 5f, top panels, arrows, and Supplementary Video 3). PLLP-KD or endocytosis inhibitor-treated 3D-MDCK cells fail to segregate Crb3 later to the tight junctions (Fig. 5f, middle and bottom panels, Supplementary Videos 4 and 5). Moreover, PLLP overexpression is sufficient to induce Crb3 endocytosis and downmodulation (Fig. 5g–i). Our results suggest that PLLP expression is necessary and sufficient to control Crb3 levels directly through regulation of apical endocytosis.

Notch signalling is required for absorptive intestinal cell differentiation across evolution[25,28,29] and the Stx7 homologue, *avl*, is required for Notch signalling in *Drosophila*[30]. PLLP-KD or EpsR-KD reduces activated Notch (NICD) levels by 60 and 40% respectively (Fig. 6a) and PLLP-KD inhibits full-length Notch1a localization in endosomes (Fig. 6b, arrows), whereas the overexpression of PLLP–GFP is sufficient to induce Notch1a internalization. These results suggested that PLLP is required for Notch-receptor endocytosis and activation. However, Notch activation also requires Epsin-mediated endocytosis of Notch ligands[31,32]. To further analyse whether PLLP and EpsR are required for receptor or ligand activation, we cultured Notch1a-expressing MDCK cells over mesenchymal OP9 cell layers stably expressing Jagged-1 (also known as Serrate) or Delta-like 1, the main ligands expressed in the zebrafish gut[33]. PLLP-KD and EpsR-KD inhibited Notch1 transactivation specifically by Jagged-1, and not by Delta-like1 (Fig. 6c–e and Supplementary Fig. 4D). Then, we co-cultured Notch1-expressing MDCK cells with Jagged-1-MDCK cells, and confirmed that Notch-receptor cells require the expression of both PLLP and EpsR, whereas EpsR expression seems to be also required in the ligand-presenting cells (Supplementary Fig. 4E–H). These results indicate that PLLP is induced in Notch-receptor cells to specifically regulate Notch activity in these cells.

Next, we analysed Notch signalling *in vivo*. The *pllp*^{pd1116} mutants present a reduced number of terminally differentiated vacuolated cells and a threefold increase of PAS-positive mucosecretory cells (Fig. 6f,g). Moreover, *pllp*^{pd1116} mutants show a marked decrease in expression of the *bona fide* Notch-effector gene *her15* (Fig. 6h), similarly to what has been previously reported for Mindbomb (*mib*) mutations, in which Jagged-family ligands are unable to signal to Notch-positive cells[33]. Together, these results indicate that Pllp is required for Notch signalling, terminal differentiation of posterior gut enterocytes and inhibition of secretory cell differentiation in the posterior midgut. To analyse whether Notch signalling is required for terminal differentiation of the posterior vacuolated IECs, we gavaged 144 hpf Mindbomb *mib1*^{ta52b} mutant larvae and Notch inhibitor-treated larvae. Both exhibited a significant reduction in the number of endocytic cells and the size of endosomes (Fig. 6i, arrows). Together, these experiments indicate that Pllp controls Notch activity, which is essential for absorptive enterocyte terminal differentiation in the posterior midgut.

DISCUSSION

Here, we characterized a developmentally regulated mechanism to induce apical endocytosis through the regulation of SNARE sorting that is necessary for epithelial morphogenesis (Fig. 6j). We propose that endosomal SNAREs are polarized to different endosomal networks at the apical and basolateral domains. Apical SNARE sorting is controlled to regulate the rate of apical protein endocytosis, involved in receptor degradation and signalling. We describe that expression of a previously uncharacterized protein, PLLP, induces SNARE recycling through its interaction with the membrane-tubulating clathrin adaptor EpsR (Fig. 6j).

In addition, our experiments demonstrate that PLLP is induced in a time- and space-specific manner to regulate the *in vivo* differentiation of a notch-mediated highly endocytic absorptive cell population in the zebrafish midgut (Fig. 6j). Epithelial morphogenesis is a finely regulated process in which epithelial cells conduct a delicate balancing act between differentiation and proliferation that becomes deregulated in different types of human carcinoma[34]. Epithelial cell differentiation greatly depends on the establishment of cellular junctions and polarity complexes that serve to organize the physiology of mature epithelial tissues. These polarity complexes, such as the Crb complex, crosstalk with proliferation pathways, such as the Notch pathway, to prevent overgrowth and, at the same time, to provide a functional population of highly differentiated epithelial cells[4]. Our experiments indicate that PLLP fine-tunes Notch signalling for differentiation of posterior gut absorptive cells. Adult *pllp* mutants presented posterior guts that resembled more anterior compartments, with a reduced population of vacuolated cells and increased populations of mucosecretory cells (Fig. 6j).

Pllp is also expressed in several other epithelial-like cell types in zebrafish not described here, such as a subpopulation of skin cells, the sheath cells of the notochord, and the neuromasts of the lateral line. Interestingly, asymmetric proliferation and differentiation of these cell types also depend on Notch signalling[35–37]. Further studies will be directed to understanding the role of PLLP in fine-tuning Notch activity during development of these organs. □

METHODS

Methods and any associated references are available in the online version of the paper.

Note: Supplementary Information is available in the online version of the paper

ACKNOWLEDGEMENTS

We thank C. M. Ruiz-Jarabo for her comments on the manuscript and members of the Martin-Belmonte laboratory and Bagnat laboratories for helpful discussions. We thank A. Alvers (Duke University, North Carolina, USA) for helping in the isolation of gut cells, J. Cocchiaro and L. Marjoram (Duke University, North Carolina, USA) for help in gavaging experiments, B. Margolis (University of Michigan, Michigan, USA) for the Crb3/panCrb antibody, R. Jahn (Max Planck Institute for Biophysical Chemistry, Germany) for Stx7 plasmids, M. Robinson (University of Cambridge, UK) for EpsR plasmids, and R. Kopan and J. L. de la Pompa (CNIC, Spain) for Notch plasmids and *mib1*^{ta52b} embryos. We also thank M. Guerra at the EM Unit for skillful technical assistance. This work was supported by grants from the MINECO (BFU2011-22622) and CONSOLIDER (CSD2009-00016) to F.M-B, by grant SAF2013-44857-R to M.L.T. by NIH innovator grant 1DP2OD006486 to M.B., and by grant AGL2013-48998-C2-2-R to G.A. A.E.R-F was supported by a CSIC JAE PhD fellowship. M.B-F. is a recipient of a Fundación Obra Social 'La Caixa' PhD fellowship. G.A. was supported by the Amarouto Program for senior researchers from the Comunidad Autónoma de Madrid.

AUTHOR CONTRIBUTIONS

A.E.R-F., M.B. and F.M-B. designed the experiments; A.E.R-F., J.B., M.B-F. and G.A. carried out the experiments; A.E.R-F. and F.M-B. wrote the manuscript; G.B. and F.P. designed and constructed RUSH experimental tools; M.J.G-L. and M.L.T. designed and constructed the Notch-ligand tools; N.R-R., M.A.A. and J.M. produced and characterized the mammalian PLLP antibody; A.E.R-F. and G.A. designed and carried out the electron microscopy experiments.

COMPETING FINANCIAL INTERESTS

The authors declare no competing financial interests.

Published online at www.nature.com/doifinder/10.1038/ncb3106
Reprints and permissions information is available online at www.nature.com/reprints

1. Rodriguez-Boulan, E. & Macara, I. G. Organization and execution of the epithelial polarity programme. *Nat. Rev. Mol. Cell Biol.* **15,** 225–242 (2014).
2. Eaton, S. & Martin-Belmonte, F. Cargo sorting in the endocytic pathway: a key regulator of cell polarity and tissue dynamics. *Cold Spring Harb. Perspect. Biol.* **6** (2014).
3. Fabrowski, P. *et al.* Tubular endocytosis drives remodelling of the apical surface during epithelial morphogenesis in *Drosophila*. *Nat. Commun.* **4,** 2244 (2013).
4. Richardson, E. C. & Pichaud, F. Crumbs is required to achieve proper organ size control during Drosophila head development. *Development* **137,** 641–650 (2010).
5. Lu, H. & Bilder, D. Endocytic control of epithelial polarity and proliferation in *Drosophila*. *Nat. Cell Biol.* **7,** 1232–1239 (2005).
6. Bokel, C. & Brand, M. Endocytosis and signaling during development. *Cold Spring Harb. Perspect. Biol.* **6** (2014).
7. Bagnat, M., Cheung, I. D., Mostov, K. E. & Stainier, D. Y. Genetic control of single lumen formation in the zebrafish gut. *Nat. Cell Biol.* **9,** 954–960 (2007).
8. Alvers, A. L., Ryan, S., Scherz, P. J., Huisken, J. & Bagnat, M. Single continuous lumen formation in the zebrafish gut is mediated by smoothened-dependent tissue remodeling. *Development* **141,** 1110–1119 (2014).
9. Sanchez-Pulido, L., Martin-Belmonte, F., Valencia, A. & Alonso, M. A. MARVEL: a conserved domain involved in membrane apposition events. *Trends Biochem. Sci.* **27,** 599–601 (2002).
10. Navis, A., Marjoram, L. & Bagnat, M. Cftr controls lumen expansion and function of Kupffer's vesicle in zebrafish. *Development* **140,** 1703–1712 (2013).
11. Cocchiaro, J. L. & Rawls, J. F. Microgavage of zebrafish larvae. *J. Visualized Experiments: JoVE* e4434 (2013).
12. Cermak, T. *et al.* Efficient design and assembly of custom TALEN and other TAL effector-based constructs for DNA targeting. *Nucleic Acids Res.* **39,** e82 (2011).
13. Golachowska, M. R., Hoekstra, D. & van, I. S. C. Recycling endosomes in apical plasma membrane domain formation and epithelial cell polarity. *Trends Cell Biol.* **20,** 618–626 (2010).
14. Galvez-Santisteban, M. *et al.* Synaptotagmin-like proteins control the formation of a single apical membrane domain in epithelial cells. *Nat. Cell Biol.* **14,** 838–849 (2012).
15. Saint-Pol, A. *et al.* Clathrin adaptor epsinR is required for retrograde sorting on early endosomal membranes. *Dev. Cell* **6,** 525–538 (2004).
16. Mills, I. G. *et al.* EpsinR: an AP1/clathrin interacting protein involved in vesicle trafficking. *J. Cell Biol.* **160,** 213–222 (2003).
17. Hirst, J., Motley, A., Harasaki, K., Peak Chew, S. Y. & Robinson, M. S. EpsinR: an ENTH domain-containing protein that interacts with AP-1. *Mol. Biol. Cell* **14,** 625–641 (2003).
18. Miller, S. E., Collins, B. M., McCoy, A. J., Robinson, M. S. & Owen, D. J. A SNARE-adaptor interaction is a new mode of cargo recognition in clathrin-coated vesicles. *Nature* **450,** 570–574 (2007).
19. Chidambaram, S., Zimmermann, J. & von Mollard, G. F. ENTH domain proteins are cargo adaptors for multiple SNARE proteins at the TGN endosome. *J. Cell Sci.* **121,** 329–338 (2008).
20. Chidambaram, S., Mullers, N., Wiederhold, K., Haucke, V. & von Mollard, G. F. Specific interaction between SNAREs and epsin N-terminal homology (ENTH) domains of epsin-related proteins in trans-Golgi network to endosome transport. *J. Biol. Chem.* **279,** 4175–4179 (2004).
21. Leventis, P. A. *et al.* Liquid facets-related (lqfR) is required for egg chamber morphogenesis during Drosophila oogenesis. *PloS ONE* **6,** e25466 (2011).
22. Lee, J. H., Overstreet, E., Fitch, E., Fleenor, S. & Fischer, J. A. Drosophila liquid facets-Related encodes Golgi epsin and is an essential gene required for cell proliferation, growth and patterning. *Dev. Biol.* **331,** 1–13 (2009).
23. Leuchowius, K. J., Weibrecht, I., Soderberg, O. in *Current Protocols in Cytometry* (eds Robinson, J. P. *et al.*) Ch. 9 (Wiley, 2011).
24. Thompson, B. J., Pichaud, F. & Roper, K. Sticking together the Crumbs—an unexpected function for an old friend. *Nat. Rev. Mol. Cell Biol.* **14,** 307–314 (2013).
25. Fre, S., Bardin, A., Robine, S. & Louvard, D. Notch signaling in intestinal homeostasis across species: the cases of Drosophila, Zebrafish and the mouse. *Exp. Cell Res.* **317,** 2740–2747 (2011).
26. Harder, J. L., Whiteman, E. L., Pieczynski, J. N., Liu, C. J. & Margolis, B. Snail destabilizes cell surface Crumbs3a. *Traffic* **13,** 1170–1185 (2012).
27. Boncompain, G. *et al.* Synchronization of secretory protein traffic in populations of cells. *Nat. Methods* **9,** 493–498 (2012).
28. VanDussen, K. L. *et al.* Notch signaling modulates proliferation and differentiation of intestinal crypt base columnar stem cells. *Development* **139,** 488–497 (2012).
29. Van Es, J. H. *et al.* Notch/gamma-secretase inhibition turns proliferative cells in intestinal crypts and adenomas into goblet cells. *Nature* **435,** 959–963 (2005).
30. Vaccari, T., Lu, H., Kanwar, R., Fortini, M. E. & Bilder, D. Endosomal entry regulates Notch receptor activation in Drosophila melanogaster. *J. Cell Biol.* **180,** 755–762 (2008).
31. Wang, W. & Struhl, G. Distinct roles for Mind bomb, Neuralized and Epsin in mediating DSL endocytosis and signaling in Drosophila. *Development* **132,** 2883–2894 (2005).
32. Wang, W. & Struhl, G. Drosophila Epsin mediates a select endocytic pathway that DSL ligands must enter to activate Notch. *Development* **131,** 5367–5380 (2004).
33. Crosnier, C. *et al.* Delta-Notch signalling controls commitment to a secretory fate in the zebrafish intestine. *Development* **132,** 1093–1104 (2005).
34. Martin-Belmonte, F. & Perez-Moreno, M. Epithelial cell polarity, stem cells and cancer. *Nat. Rev. Cancer* **12,** 23–38 (2012).
35. Yamamoto, M. *et al.* Mib-Jag1-Notch signalling regulates patterning and structural roles of the notochord by controlling cell-fate decisions. *Development* **137,** 2527–2537 (2010).
36. Wibowo, I., Pinto-Teixeira, F., Satou, C., Higashijima, S. & Lopez-Schier, H. Compartmentalized Notch signaling sustains epithelial mirror symmetry. *Development* **138,** 1143–1152 (2011).
37. Liu, Y., Pathak, N., Kramer-Zucker, A. & Drummond, I. A. Notch signaling controls the differentiation of transporting epithelia and multiciliated cells in the zebrafish pronephros. *Development* **134,** 1111–1122 (2007).

METHODS

Plasmids. Rat Stx7–GFP plasmids were kind gifts from R. Jahn (Max Planck Institute for Biophysical Chemistry, Germany). Human Rab11a–GFP, canine PLLP–GFP and canine PLLP–Cherry were constructed by PCR and cloned into pEGFP/mCherry vectors (Clontech). The siRNA no. 2-resistant (R) variants were generated by introducing synonymous mutations with the Quikchange XLII kit (Stratagene). Canine PLLP–myc/myc–birA∗ was constructed by PCR and cloned into pCR3.1(+) (Invitrogen). Human EpsR–GFP, GST–N-EpsR and GST–C-EpsR were gifts from S. Robinson (University of Cambridge, UK). Rab7–GFP was from R. Puertollano (NIH, USA). The BAC clones containing *pllp* and *lamp2* genes were obtained from Source Biosciences (*pllp* HUKGB735N1073Q/DKEY-73N10 and *lamp2* HUKGB735N0515Q/DKEY-15N5). GFP–Crb3a were kindly provided by D. Bryant (Beatson Institute, University of Glasgow, UK). The spacer–GFP/RFP sequence was cloned by BAC homologous recombination in bacteria as previously reported[10]. Full-length Notch1a–myc was obtained from Addgene (plasmid 41728).

Antibodies and reagents. The polyclonal antibody (pAb) against mammalian PLLP (1:500 immunofluorescence (IF) on cold methanol/acetone fixation, 1:1,000 western blotting (WB)) was designed and generated in rabbits by injecting a combination of cytoplasmic peptides from the human PLLP sequence as previously described[38]. Podocalyxin/gp135 (1:500 IF, 1:1,000 WB) was a gift from G. Ojakian (State University of New York Downstate Medical Center, USA). Crb3 pAb (1:250 IF on acetone fixation, 1:1,000 WB) was a gift from B. Margolis (University of Michigan, Ann Arbor, USA). Cleaved Notch1 rabbit mAb (no. 4147, 1:1,000 WB, Cell Signaling), GAPDH mAb 6C5 (no. sc-32233, 1:1,000 WB, Santa Cruz Biotechnologies), βcatenin pAb (no. sc-7199, 1:500 IF, Santa Cruz Biotechnologies), E-cadherin mAb (rr1, 1:500 IF, DSHB), GFP mAb (no. 11814460001, 1:100 IF, 1:1,000 WB, Roche), GFP pAb (no. A-11122, 1:1,000 immunoprecipitation (IP), 1:1,000 IF, 1:2,000 WB, Life Technologies), myc 9E10 mAb (no. 11667149001, 1:1,000 IF on acetone fixation, Roche), EpsR mAb (no. 86046, 1:100 IF on methanol/acetone fixation, 1:500 WB, Abcam), Stx7 pAb (no. 110072, 1:100 on IF on acetone fixation, 1:500 WB, Synaptic Systems), Rab11 pAb (no. 715300, 1:500 IF, 1:500 WB, Life Technologies), tubulin (no. T9026, DM1A, 1:1,000 WB, Sigma-Aldrich) and EEA1 mAb (no. 610457, 1:500 IF, BD Biosciences) were used as primary antibodies. Peroxidase-conjugated antibodies were used for western blotting (Jackson Immunoresearch). Alexa405/488/555/647-conjugated phalloidin or secondary antibodies were used for immunofluorescence. DAPI, ToPRO3, Lysotracker-red and dextran–Texas red (TR) were from Life Technologies. Dynasore (MERCK) was used at 100 μM in culture medium to inhibit dynamin, and DAPT (Sigma-Aldrich) at 100 μM was used to inhibit Notch cleavage.

Transgenic animals and mutants. Zebrafish stocks were maintained at 28 °C. The zebrafish lines used were EK, *TgBAC(cldn15la-GFP)pd1034* (ref. 8), *TgBAC(pllp–GFP)pd1114*, *TgBAC(pllp–GFP)pd1115*, *TgBAC(lamp2–spRFP)pd1117*, *mib1*^{ta52b} (ref. 39) and *pllp*^{pd1116}. Zebrafish BAC lines were generated as previously described[10]. Zebrafish that were found dead, not swimming or without heartbeat were excluded from the analyses. To randomize animal selection, we followed common protocols for unbiased tank fishing. Genotypes were determined by fin clipping. Larvae and juveniles were pipetted into fixation media without preselecting them on the low-magnification scope. Except where noted, larvae were 144 hpf, juveniles were 16 dpf and adults were 4 months old. Experiments were supervised by the bioethics committee of the Centro de Biología Molecular 'Severo Ochoa' (CSIC) and performed in compliance with bioethical regulations of the European Commission. No statistical method was used to predetermine sample size for treatment groups. There was no requirement for animal randomization during the course of the animal studies.

TALEN-mediated editing. Three TALENs were designed to target the first exon of *pllp* using TALEN targeter and constructed using Golden Gate assembly into the pCS2-TAL3DD/RR vectors using the Addgene v2.0 kit[12,40]. The TALEN used to generate the *pllp*^{pd1116} mutant allele reported here was designed to target the following sequence of *Danio rerio pllp* exon1: 5′-TTGACATGGGTTTTATcaagagcattcctggaa TACTGCTTATAGCCGA-3′, and composed of the following TAL effector domains: pCS2-TAL3DD_*pllpE1* NG NN NI HD NI NG NN NN NN NG NG NG NG NI NG; pCS2-TAL3RR_*pllpE1* HD NN NN HD NG NI NG NI NI NN HD NI NN NG NI. Zebrafish were injected into the yolk at the one-cell stage with 200 pg total TALEN RNA and 100 pg of dsRed RNA to select correctly injected embryos. Mutant alleles were identified by defective BsmI digestion of the PCR product generated with the following primers: FW: 5′-CTGGGAAGGTCAGCACTCAG-3′; RV: 5′-AC GGAACAGAAAAGTGGGTGT-3′. The BsmI-undigested PCR band was T/A cloned into the pGEM-T vector for allele sequencing. The experiments shown here were performed on F4/F5 fish and larvae.

Fish gavaging. Zebrafish larvae from 144 hpf were tricained for 5 min and immersed in 3% methylcellulose. Microforged capillary needles were used to microinject 10 nl of a 1:4:1 dextran–TR/water/Phenol-red solution. Methylcellulose was washed off and fish were incubated at 28 °C for 2 h before confocal microscopy analysis or fixation.

Endocytosis assay in cells. MDCK cells stably expressing GFP–Crb3a were cultured as monolayers, washed with cold 1% FBS-supplemented MEM and placed on ice for 15 min. Then, coverslips were placed on a 100 μl drop of cold 1% FBS MEM containing a 1:10,000 dilution of the polyclonal GFP antibody at 4 °C for 30 min. Coverslips were washed 3 times with 1% FBS-supplemented MEM and placed on plates containing warm MEM and cultured at 37 ° for 90 min. Cells were washed in Ca/Mg-PBS, fixed and stained for immunofluorescence.

***In situ* hybridization.** The probe to detect the *pllp* transcript by *in situ* hybridization was PCR amplified from 5 dpf larval cDNA and ligated into pGEMT-Easy (Promega). *In situ* hybridization was performed as previously described. The plasmids were linearized and digoxygenin-labelled RNA was generated using the DIG-labelled nucleotides (Roche) and T7 polymerase (NEB). Stained embryos were imaged on a Discovery.V20 stereoscope (Zeiss) with an Achromat S 1.0 × lens.

Fish sectioning and analysis. Zebrafish embryos and larvae from different time points were fixed overnight in PBS-buffered 4% PFA (Sigma), washed twice in PBS and embedded in PBS-buffered 4% low-melt agarose blocks. Blocks were cut in 200 μm sections using a Vibratome (Leica). Sections were blocked/permeabilized with PBS-3%BSA containing 0.5% Tx100 and then incubated with the indicated antibodies. Stained sections were mounted using DAPI-Fluoromount or DAPI-Vectashield. Sectioned fish were analysed on a confocal microscope. Adult fish were paraffin embedded, sectioned in 5 μm slices, dewaxed and stained with haematoxylin/eosin (HE) or periodic acid–Schiff (PAS). Data were repeated using three different sections from the same tissue and/or genotype. Representative images are shown.

Cell culture and stable cell lines. MDCK type 2 (MDCK-II, MDCK.2) cells were obtained from ATCC and grown as described previously[41]. MDCK cells stably expressing PLLP–GFP, PLLP–Cherry, GFP–Rab7, GFP–VAMP8, GFP–Stx7 and EpsR–GFP were made by transfection using Lipofectamine 2000 (Life Technologies) and clones were selected by treating cells with G418 (0.5 mg ml^{-1}). The Notch1a–myc stable cell line was made by co-transfection with the blasticidin-resistant gene (pBlast) and selection for 10 d with 0.5 μg ml^{-1} blasticidin. Mycoplasma testing was regularly performed. To prepare cysts in Matrigel, cells were trypsinized to a single-cell suspension of 2×10^4 cells ml^{-1} in 2% Matrigel and plated in coverglass bottom chambers (IBIDI) covered with Matrigel. Cysts were grown and fixed at indicated time points.

Confocal microscopy and videomicroscopy. Immunofluorescence of cysts was previously described[41]. Fixed cells in 3D cultures were analysed mounted in ProLong Gold antifade reagent. Fixed cells in monolayers were analysed mounted in Fluoromount. Cysts were analysed on a 510 or 710 LSM confocal microscope (Carl Zeiss) using a ×63 NA 1.4 oil Plan-Apochromat objective and a ×63 NA 1.2 water C-Apochromat Corr (for live-cell and cyst imaging) and ZEN software suite (Carl Zeiss). Fish sections and whole-mounts were analysed on a SP5 confocal microscope (Leica) with a ×10/0.40 HC PL APO air objective, a ×20/0.70 HC PL APO oil objective, and a ×40 /1.25–0.75 HCX PL APO oil objective, using Application Suite software (Leica). For image processing, we used FIJI/ImageJ (National Institutes of Health). For videomicroscopy and 3D reconstitutions, we processed maximum *z*-projections of all stacks using ImageJ software. For quantification of lumen formation, MDCK cysts with a single actin/Podxl staining at the interior surface and β-catenin facing the ECM were identified as normal lumina. We excluded cyst formation experiments that presented lower than 50% normal lumen formation (at 48 h) or 60% (at 72 h). Cysts at 72 h presenting two large lumina were considered 'normal'. To randomize cyst or cell counting, we randomly selected fields using low magnification, and then counted or took images at higher magnification for measurements. Immunofluorescence experiments in cell lines were performed three independent times and images shown are representative from samples that were used for quantification. For fluorescence intensity quantification in MDCK cysts, background was removed, maximum projections of optimal volumetric slicing of single cells were obtained and fluorescence signal was quantified as total integrated density per cell. For GFP–Stx7 or Rab11 signal polarization quantification, perpendicular linear intensity profiles were measured. For Crb measurements in zebrafish, apical membrane regions (1 μm × 3 μm rectangle) were chosen and measured from 10 cells per fish section.

DOI: 10.1038/ncb3106

RUSH assay. The RUSH protocol was performed as previously described, with the following modifications. MDCK cysts stably expressing GFP–SBP–Crb3a and streptavidin-KDEL were grown in Mattek coverglass bottom plates for 72 h, washed and incubated with 10 mM Hepes-buffer, 1% serum-supplemented phenol-red-free MEM and imaged using a 510 LSM confocal microscope (Zeiss). Biotin-supplemented MEM (40 μM) was added at $t = 0$ when image acquisition started. For endocytosis inhibitor experiments, cysts were treated with 100 μM dynasore at 40 min after biotin addition, when most Crb3 protein had reached the apical surface.

Electron microscopy. For BSA–gold endocytosis TEM, 144 hpf larvae were gavaged with 15 nm gold-conjugated BSA (EM Laboratory, Utrecht University) supplemented with dextran–TR for 2 h. Then, larvae were fixed in 2% (w/vol) PFA, 2% (w/vol) glutaraldehyde in 0.1 M phosphate buffer (PB, at pH 7.4) for 2 h at room temperature and overnight at 4 °C. Subsequently, posterior midgut sections were embedded in Epon resin, sectioned using a ultramicrotome (Ultracut E, Leica), and stained with uranyl acetate and lead citrate and imaged at 80 kV using a JEM1010 Jeol microscope. For immunogold electron microscopy, 144 hpf zebrafish larvae were fixed in 2% (w/vol) PFA and 0.2% (w/vol) glutaraldehyde in 0.1 M phosphate buffer (PB, at pH 7.4) for 2 h at room temperature and kept in 1% (w/vol) PFA in PB at 4 °C. Subsequently, posterior gut sections were embedded in 10% (w/vol) gelatine, and processed for cryosectioning. Guts were sectioned along the apicobasal axis on an EM FCS cryo-ultramicrotome (Ultracut UCT, Leica) at −120 °C. For immunogold labelling, thawed 75-nm-thick cryosections were incubated with rabbit anti-GFP (1:500, Life Technologies) followed by protein A conjugated to 15-nm gold particles (EM Laboratory, Utrecht University). Sections were stained with a mix of 1.8% methylcellulose and 0.4% uranyl acetate and imaged at 80 kV using a JEM1010 Jeol microscope and a 4×4 k CMOS F416 camera from TVIPS (Gauting).

RNAi and western blot. Twenty-five nucleotide stealth siRNA duplexes targeting mRNA sequences of canine PLLP and Stx7 were purchased from Life Technologies. Twenty-five nucleotide siRNA duplexes targeting EpsR were purchased from Sigma-Aldrich using dTdT overhangs. Sequences were submitted to BLAST search to ensure targeting specificity and minimize off-targets. MDCK cells were transfected using AMAXA Nucleofector-II equipment, reagents and protocols (Lonza). Cells were transfected with 10 μl of siRNA (200 μM), plated in 6-well plates, cultured for 24 h, trypsinized and then plated to grow cysts for the indicated time points. Total cell lysates were analysed by western blotting. Immunoblots shown are representative of experiments that were repeated and reproduced at least three independent times. For some challenging experiments and antibodies, the representative blots are ones that show the least nonspecific background and have a low signal-to-noise ratio.

The siRNAs targeted the following sequences: control: 5′-CCUUCGGGUGGAA CAUGCUCUCUUU-3′ PLLP no. 1: 5′-CUGCUGCAGCUGGUGCUGGGGCUG C-3′ PLLP no. 2: 5′-CCUCUGGCUGGUGACAAUCGUCUUU-3′ PLLP no. 3: 5′-C CUAAGGAAUCGGGAUCCUUCCUCU-3′ EpsR no. 1: 5′-CCUAUGAAUGUGA UGACCCAAAGUU-3′, EpsR no. 2: 5′-CAUGAACAUAGGGAUGUCAACUGCU-3′, EpsR no. 3: 5′-AAGGAGCAGAUUGAAUGAAGGAUUU-3′, Stx7 no. 1: 5′-UUC AGGUGAAUCUUGAGGUGUUCCA-3′ Stx7 no. 2: 5′-CAGAAGAUGACCUCC GCCUUAUUCA-3′ Stx7 no. 3: 5′-UAGAGAAUGUAGUGCAAUAGUGUGC-3′.

Probe ligation assay. The probe ligation assay (O-LINK) was performed using anti-PLLP (rabbit polyclonal) and anti-GFP (mouse, Roche) according to the manufacturer's instructions.

***In vivo* biotinylation of PLLP-proximal proteins.** MDCK cells stably expressing the promiscuous mutant (R118G) of the humanized bacterial biotin-ligase (birA∗) or canine PLLP–myc/myc–birA∗ constructs were incubated with 50 μM biotin for 16 h and lysed using 4% SDS, and biotinylated peptides were purified using streptavidin-coated magnetic beads (Genscript). The bioID technique was performed as previously described[42] and eluted peptides were analysed by liquid chromatography tandem mass spectrometry and peptide-mass fingerprinting, considering up to 2 biotinylations per peptide, in collaboration with the Proteomics unit at Centro Nacional de Biotecnología (CSIC).

Pulldowns. The full-length EpsR construct is extremely protease sensitive, so the NH2-terminal ENTH domain (amino acids 1–165) and the COOH-terminal domain (amino acids 165–625) of human EpsR were expressed separately as previously published[17]. GST-fusion constructs were transformed into BL21 *Escherichia coli* and expressed by incubating bacterial clones at 30 °C using 0.5 mM IPTG overnight. Bacterial cultures were collected and lysed at 10,000 psi using a French-press in cold-PBS buffer containing protease inhibitor cocktail (Sigma-Aldrich). Bacterial lysates were incubated with GSH–Sepharose beads (GE Amersham) and beads were washed 5 times in PBS before use. MDCK cysts (10^7) grown for 72 h were washed twice in cold PBS and lysed in 1 ml of TNE buffer (50 mM Tris, 250 mM NaCl, 10 mM EDTA, pH 7.4) containing 0.1% NP-40 and protease inhibitor cocktail (Sigma-Aldrich). Each 1 ml of MDCK cyst lysate was incubated with beads containing 100 μg of GST–EpsR (N or C-terminal domains) or GST alone (control) for 2 h. Beads were washed in TNE buffer 5 times, dried by aspiration and eluted in 100 μl of Laemmli buffer (LB) and analysed by western blotting. We performed experiments at least three independent times to be confident in the experimental reproducibility.

Co-immunoprecipitation. MDCK cells (10^7) stably expressing PLLP–GFP or EpsR–GFP were grown for 72 h, washed once in cold PBS and lysed in 1 ml of TNE buffer (50 mM Tris, 150 mM NaCl, 10 mM EDTA, pH 7.4) containing 0.5% Triton-X100 and protease inhibitor cocktail (Sigma-Aldrich). Each 1 ml of MDCK cyst lysate was incubated with 2 μg of purified polyclonal anti-GFP (Life Technologies) or 2 μg of rabbit antiserum (control). Beads were washed in TNE buffer 5 times, dried by aspiration and bound proteins were eluted in 100 μl of LB and analysed by western blotting. We performed experiments at least three independent times to be confident in the experimental reproducibility.

Notch-ligand retroviral transduction. pLZRS-IRES-eGFP retroviral constructs either empty or encoding human Delta-like1 or Jagged1 (kindly provided by S. Parreira, Instituto de Histologia e Embriologia, Lisboa, Portugal) were transfected into the packaging 293T Phoenix-Amphotropic cell line (kindly provided by G. Nolan, Stanford University, Stanford, California, USA). Retroviral supernatants obtained from puromycin-selected transfected cells were used for transduction of MDCK and OP9 (ATCC) cells by centrifugation in the presence of Polybrene. Transduced OP9 and MDCK GFP+ cells were isolated by cell sorting (FACSVAntage) 48 h post-transduction.

Notch activity assays. MDCK cells (10^6) stably expressing murine Notch1a–myc were cultured for 48 h in cysts and western blotting was performed to quantify the cleaved Notch1a band at Val 1744 (relative molecular mass 75,000). For transactivation assays on OP9 layers, first OP9 cells were transduced with IRES–EGFP, Jagged1–IRES–EGFP or Delta-like1–IRES–EGFP retroviral supernatants prepared in 293-T Phoenix-Ampho cells and FACS-sorted to select a GFP^+ population. OP9 cells were passaged with 20%FBS-supplemented nucleotide-free αMEM (Gibco, Life Technologies). GFP^+ OP9 cells (10^5) were seeded on P35 plates and allowed to attach for 2 h at 37° in a CO_2-incubator. Then, Notch1-MDCK cells (10^6) were seeded on top of the OP9 layer, and grown for 48 h. For MDCK/MDCK transactivation assays, MDCK-II cells were transduced with IRES–EGFP or Jagged1–IRES–EGFP retroviral supernatants and FACS-sorted to select a GFP^+ population. Notch1-MDCK cells and Jagged1-MDCK cells were mixed 4:1 in 2 ml 2%MG in MEM (at 100,000 cells ml^{-1}) and seeded in Matrigel-coated P35 plates. In all cases, co-cultures were incubated for 48 h and analysed by western blotting.

Real-time quantitative PCR. Quantitative analysis of gene expression was carried out by real-time quantitative PCR. RNAs were purified from cells or zebrafish guts using the RNAeasy kit (Qiagen) to eliminate genomic DNA contamination. RNA was converted into cDNA using the RNA-to-cDNA High capacity kit and then qPCR was performed using the ABI-PRISM 7900HT SDS system (Applied Biosystems). PCRs were performed on 10 ng template cDNA per well using intron-spanning primers. Specificity was BLAST-analysed for each primer pair, and we performed a melting curve analysis to ensure that a single PCR product was generated.

Morpholino injections. Morpholinos targeting *pllp* were designed, prepared and injected according to the manufacturer's instructions (Genetools, LLC). We injected 4 ng per one-cell embryo in a 1:1:1 dilution with water and Phenol red. The morpholino sequences were: *pllp* AUG-MO (MO1): 5′-ACCTTCCCAGGAAAATC CGCCATTT-3′ *pllp* SPL-MO (MO2): 5′-GAATAGTCAAAGAGTCTCACCA CCA-3′.

Statistical analysis. Effect size of 2.4 or greater was expected on the basis of previous publications using the same experimental approaches (that is, acute gene disruption using mutants or RNAi). We chose an appropriate sample size in each experiment to ensure 0.80 statistical power and a significance level of 0.05. G-Power software was used to predict sample size. Data were then reanalysed *post hoc* to measure effect size and validate the *t*-tests. In some challenging experiments, certain data sets were not able to reach ideal sample sizes, and we do not provide a *P* value. We used Student's *t*-test for measuring *P* values. Significance level was set at 0.05. For small data sets, normal distribution was predicted from pooled data derived from previous similar experimental approaches (RNAi experiments, cyst formation quantification). For large data sets, we verified normal distribution using χ^2. In cases where variance was conspicuously different between two treatments Levene's test was used to verify

homoscedasticity. Investigators were not blinded to allocation during experiments and outcome assessment.

38. Bosse, F., Hasse, B., Pippirs, U., Greiner-Petter, R. & Muller, H. W. Proteolipid plasmolipin: localization in polarized cells, regulated expression and lipid raft association in CNS and PNS myelin. *J. Neurochem.* **86,** 508–518 (2003).
39. Schier, A. F. *et al.* Mutations affecting the development of the embryonic zebrafish brain. *Development* **123,** 165–178 (1996).
40. Doyle, E. L. *et al.* TAL Effector-Nucleotide Targeter (TALE-NT) 2.0: tools for TAL effector design and target prediction. *Nucleic Acids Res.* **40,** W117–W122 (2012).
41. Rodriguez-Fraticelli, A. E. *et al.* The Cdc42 GEF Intersectin 2 controls mitotic spindle orientation to form the lumen during epithelial morphogenesis. *J. Cell Biol.* **189,** 725–738 (2010).
42. Roux, K. J., Kim, D. I., Raida, M. & Burke, B. A promiscuous biotin ligase fusion protein identifies proximal and interacting proteins in mammalian cells. *J. Cell Biol.* **196,** 801–810 (2012).